Fuel 280 (2020) 118657

Contents lists available at ScienceDirect

Fuel

journal homepage: www.elsevier.com/locate/fuel

Full Length Article

# A numerical study of a compression ignition engine operating with constant volume combustion phase: Effects of constant volume phase on combustion performance and emissions

C.J. Ramsay[a], K.K.J. Ranga Dinesh[a,*], W. Fairney[b], N. Vaughan[b]

[a] Energy Technology Research Group, Faculty of Engineering and the Environment, University of Southampton, Southampton SO17 1BJ, UK
[b] Covaxe Ltd, Hawkesbury Upton, South Gloucestershire GL9 1AY, UK

ARTICLE INFO

*Keywords:*
Compression ignition engine
Constant volume combustion
Engine performance
Emission reduction methods
Numerical modelling

ABSTRACT

A detailed numerical study is carried out to investigate the performance of a turbocharged compression ignition engine operating under a novel combustion strategy in which fuel injection and most of the combustion occur at a constant volume. Simulations have been performed using URANS based modelling approach along with several other sub-models. A detailed validation of the CFD model has been carried out using data from a conventional crank engine.

A parametric study has been performed to investigate the effects of the duration and timing of the constant volume combustion phase (CVCP) on the engine's thermal efficiency and emissions, with comparisons against the conventional engine. Much higher in-cylinder pressures and temperatures are observed in the CVCP strategy.

The results demonstrate that the CVCP strategy is capable of yielding reduced gross indicated specific fuel consumptions of up to 20% and far lower $CO_2$ and soot emissions but incurs unacceptable increase to nitrogen oxide emissions. However, it was found that a combination of exhaust gas recirculation and improved fuel injection methods can counter the increased nitrogen oxide emissions under the CVCP strategy, while still maintaining the improved engine performance and low carbon-based emissions.

## 1. Introduction

Compression ignition (CI) engines fuelled by diesel play a vital role in many heavy duty transport, power generation and agricultural applications due to superior torque, greater power output, higher thermal efficiency, better fuel economy and reliability compared to spark ignition (SI) engines [1,2]. The greater power output, higher thermal efficiency and better fuel economy of CI engines are achieved through higher compression ratio, greater air to fuel ratio, load control through direct fuel injection, rapid combustion process and lower breathing and pumping loses [1]. However, due to the nature of combustion in CI engines high temperatures and uneven distributions of fuel lead to higher levels of harmful gaseous emissions such as nitrogen oxides ($NO_x$), carbon monoxide (CO) and soot [3]. As a result, conventional CI engines face new challenges to keep up with increasingly strict emissions and fuel consumption regulations [4]. Current European Union regulations limit new heavy duty diesel vehicles to 0.4 g/kWh of $NO_x$ production and 0.01 g/kWh of soot production [5], with these standards set to become more stringent in the future. The simultaneous reduction of both $NO_x$ and soot in a CI engine is a challenging issue, and generally boils down to a trade-off between the two, whereby, higher combustion temperatures lead to higher $NO_x$ formation but lower temperatures to higher soot [6].

A number of advanced engine design approaches have the potential to lower emissions and increase fuel efficiency [7]. Low temperature combustion (LTC) strategies including homogeneous charge compression ignition (HCCI) [8], premixed charge compression ignition [9], and reactivity controlled compression ignition [10] all show promise in reducing emissions while maintaining performance but require complex operational and control processes [11]. Exhaust gas recirculation (EGR) is another addition which can significantly reduce $NO_x$ emissions while having minimal impact on performance [12]. Utilisation of alternative green fuels has the potential to reduce pollutant emissions while maintaining performance and reducing fossil fuel consumption. These include liquid fuels/additives such as biodiesel [13], ethanol [14], methanol [15], butanol [16], and gaseous fuels such as natural gas [17] and hydrogen [18] under dual-fuel combustion strategies. Alternative engine operating cycles such as the over-expanded [19,20], split [21],

* Corresponding author.
*E-mail address:* dinesh.kahanda-koralage@soton.ac.uk (K.K.J. Ranga Dinesh).

https://doi.org/10.1016/j.fuel.2020.118657
Received 10 April 2020; Received in revised form 4 June 2020; Accepted 6 July 2020

**Nomenclature**

| | |
|---|---|
| BDC | bottom dead centre |
| CI | compression ignition |
| CVCP | constant volume combustion phase |
| CFD | computational fluid dynamics |
| CA | crank angle |
| CO | carbon monoxide |
| EVO | exhaust valve open |
| deg | degree |
| EGR | exhaust gas recirculation |
| HRR | heat release rate |
| HCCI | homogeneous charge compression ignition |
| IVC | inlet valve close |
| $NO_x$ | nitrogen oxide |
| LTC | low temperature combustion |
| PISO | pressure-implicit with splitting of operators |
| RCCI | reactivity controlled compression ignition |
| PCCI | premixed charged compression ignition |
| RPM | revolutions per minute |
| TDC | top dead centre |
| UHC | unburned hydro carbon |
| URANS | unsteady Reynolds-Averaged Navier-Stokes |
| $CO_2$ | carbon dioxide |
| CV | constant volume |

Wankel [22] and free piston [23] offer varying benefits with regards to performance and emissions reductions and can potentially be used in conjunction with the aforementioned combustion strategies and alternative fuels.

One of the major operating points of conventional internal combustion engines is the piston dwelling near top dead centre (TDC) which increases the time allowed for combustion. Further increasing this dwell time has the potential to improve the quality of combustion and therefore increase performance while simultaneously reducing the output of harmful pollutant emissions such as soot and unburned hydrocarbons. In theory the most efficient cycle for a given internal combustion engine is the Otto cycle which consists of 1) isentropic compression, 2) constant volume heat addition, 3) isentropic expansion and 4) constant volume heat rejection [24]. Practical CI engines fail to provide the ideal Otto cycle, largely due to the lack of combustion occurring at a constant volume [25]. Conventional engines use simple crank-slider mechanisms to convert linear work to rotational torque which means that the piston can only move between TDC and bottom dead centre (BDC) at a frequency proportional to engine speed. Combustion however occurs over a fixed period and is largely unaffected by engine speed. Any combustion occurring before TDC incurs negative work and combustion occurring during the expansion does not reach its maximum thermal potential due to reductions in pressure and temperature as the piston moves away from TDC - combustion is not occurring at a constant volume. Reducing piston velocity at TDC while increasing velocity during the expansion and or compression stroke to maintain average engine speed would allow for a greater amount of constant volume combustion.

Chen et al. [25] designed and tested a “Quasi-constant volume” SI engine where an electric motor/generator directly controlled piston trajectories and rotational velocities. Through reduced velocities of the piston near TDC increases in work by 11% were observed compared to conventional operation. Dorić et al. [26] modelled a SI engine which combined variable compression ratio and engine displacement to allow for increased levels of constant volume combustion due to slower movement of the piston at TDC and BDC. Significant improvements to performance were observed for part-load conditions and moderate improvements at full load. Variable compression ratio engines in general show promise as they can be tailored to the given cycles operating conditions [27]. Zhang et al. [28] modelled a free piston engine with asymmetric piston trajectory controls to reduce $NO_x$, CO and UHC emissions and improve thermal efficiency by increasing piston dwell time near TDC. Similar modelling was also carried out by the same group which showed the applicability of the piston trajectory control to the likes of HCCI and combustion of alternative fuels [29,30].

This paper focuses on computational fluid dynamics (CFD) modelling of an engine cycle which implements a full constant volume combustion phase (CVCP) in a CI engine. The objective of this numerical study is threefold: (1) to investigate the effects of CVCP start time on engine performance and pollutant emissions; (2) to examine the effects CVCP duration on engine performance and emissions; (3) to study the emission reduction methods under the CVCP strategy.

Fig. 1 shows a comparison of the pressure-volume diagrams for an Otto cycle, a conventional engine cycle and the proposed CVCP cycle, each at the same compression ratio, where area between the curves gives the net work output.

In the present study, an experimental configuration of a recently built four-stroke turbocharged diesel direct injection CI engine from Tsujimura et al. [31] was modelled to validate the CFD modelling strategy for the conventional diesel cycle where fuel injection occurs when the piston is near TDC and then combustion with normal reciprocating motion (see conventional cycle in Fig. 1). Then the conventional engine configuration of Tsujimura et al. [31] was theoretically/numerically modified by changing the piston profile to simulate the proposed CVCP cycle (see CVCP cycle in Fig. 1). In all CVCP test cases, fuel injection and combustion occur at TDC. The ultimate goal of the present numerical study is to identify the best possible theoretical values for CVCP start time, CVCP duration and best possible emissions reduction method for CVCP operation. The findings of this parametric study will be used to optimise a novel 2-stroke opposed piston CVCP CI engine configuration currently being developed by Covaxe Group [32]. For example, Fig. 2 shows the prototype opposed piston axial engine configuration in which fuel injection and combustion occurs at a constant volume. As seen in Fig. 2, the initial design of the engine consists of opposed pistons which drive two cams mounted directly on the main drive shaft. The pistons meet at TDC where fuel is injected and combustion takes place. The cams are profiled so as to hold the pistons together at TDC for the duration of fuel injection until combustion is virtually completed. The engine is designed to run under the CVCP cycle (see Fig. 1) with the aim to improve thermal efficiency due to higher in-cylinder pressures and temperatures, and reduce carbon-

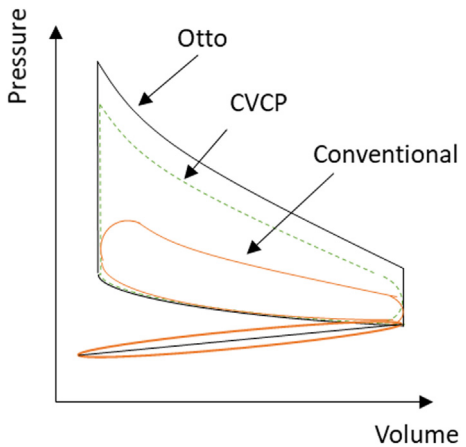


**Fig. 1.** Pressure-Volume diagram for Ideal Otto, CVCP and conventional engine cycles at a given compression ratio.

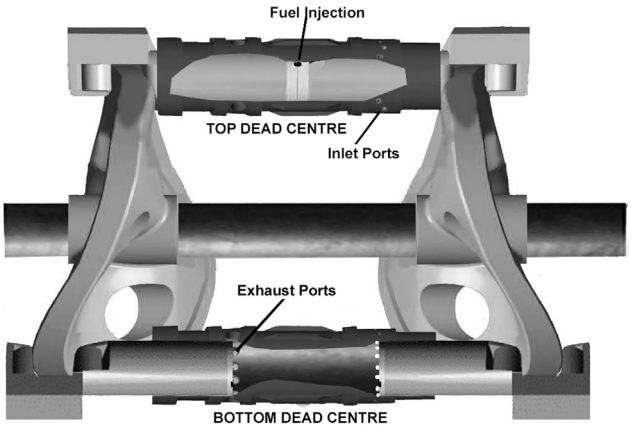


**Fig. 2.** Schematic of the prototype two stroke opposed piston CI engine configuration designed to run using the CVCP cycle, where combustion occurs at TDC [32].

based emissions due to higher quality of combustion compared to a conventional cycle.

The remainder of the paper is organised as follows: section 2 describes the numerical model set up, simulation methodology and validation, section 3 describes the results and discussion followed by conclusions in section 4.

## 2. Numerical methodology and modelling setup

The numerical simulations were carried out from inlet valve close (IVC) to exhaust valve open (EVO) using three-dimensional unsteady Reynolds Averaged Navier-Stokes (URANS) approach. The simulations were carried out using commercial CFD software Fluent 19.1. All simulations were performed on the University of Southampton IRIDIS 4 high performance computing cluster.

### 2.1. Governing equations and modelling

The modelling framework solved incompressible URANS equations for mass, momentum, energy and transport equations for the mean mixture fraction and mean mixture fraction variance in the main solver for a chemically reacting mixture using the finite volume method.

Mass:

$$\frac{\partial \rho}{\partial t} + \frac{\partial \rho \bar{u}_j}{\partial x_j} = S_m, \tag{1}$$

Momentum:

$$\frac{\partial \rho \bar{u}_i}{\partial t} + \frac{\partial \rho u_i \bar{u}_j}{\partial x_j} = -\frac{\partial \bar{P}}{\partial x_i} + \frac{\partial}{\partial x_j}\left(\mu\left(\frac{\partial \bar{u}_j}{\partial x_i} + \frac{\partial \bar{u}_i}{\partial x_j} - \frac{2}{3}\delta_{ij}\frac{\partial \bar{u}_k}{\partial x_k}\right)\right) - \frac{\partial \rho u'_i \bar{u'}_j}{\partial x_j} + S_i, \tag{2}$$

Energy:

$$\frac{\partial \rho \bar{H}}{\partial t} + \frac{\partial \rho \bar{u}_j \bar{H}}{\partial x_j} = \frac{\partial}{\partial x_j}\left(\frac{k_{eff}}{C_p}\frac{\partial \bar{H}}{\partial x_j}\right) + S_h, \tag{3}$$

Mixture Fraction:

$$\frac{\partial \rho \bar{f}}{\partial t} + \frac{\partial \rho \bar{u}_j \bar{f}}{\partial x_j} = \frac{\partial}{\partial x_j}\left(\left(\frac{\mu}{\sigma} + \frac{\mu_t}{\sigma_t}\right)\frac{\partial \bar{f}}{\partial x_j}\right) + S_{m,i}, \tag{4}$$

Mixture Fraction Variance:

$$\frac{\partial \rho \bar{f}'2}{\partial t} + \frac{\partial \rho \bar{u}_j \bar{f}'2}{\partial x_j} = \frac{\partial}{\partial x_j}\left(\left(\frac{\mu}{\sigma} + \frac{\mu_t}{\sigma_t}\right)\frac{\partial \bar{f}'2}{\partial x_j}\right) + C_g \mu_t \left(\frac{\partial \bar{f}}{\partial x_j}\right)^2 - C_d \rho \frac{\varepsilon}{k}\bar{f}'2. \tag{5}$$

The nitric oxide and soot emissions were calculated by solving the transport equations at a post-processing stage as this method was found to be computationally more efficient.

The transport equation for $NO_x$ mass fraction, $Y_{NO}$, is given by:

$$\frac{\partial \rho \bar{Y}_{NO}}{\partial t} + \frac{\partial \rho \bar{u}_j \bar{Y}_{NO}}{\partial x_j} = \frac{\partial}{\partial x_j}\left(\rho D \frac{\partial \bar{Y}_{NO}}{\partial x_j}\right) + S_{NO}, \tag{6}$$

A one-step Khan and Greeves soot model [33] was employed to calculate the soot formation. This model solves a single transport equation for the soot mass fraction, $Y_{soot}$:

$$\frac{\partial \rho \bar{Y}_{soot}}{\partial t} + \frac{\partial \rho \bar{u}_j \bar{Y}_{soot}}{\partial x_j} = \frac{\partial}{\partial x_j}\left(\frac{\mu_t}{\sigma_{soot}}\frac{\partial \bar{Y}_{soot}}{\partial x_j}\right) + R_{soot}, \tag{7}$$

where $\rho$is the density of the fluid, $t$ is time, $\bar{u}_j$ a component of the mean velocity vector, $u'_j$ a component of the fluctuating velocity vector, $x_j$ a component of the position vector, $S_m$ the source term accounting for any mass added by fuel spray, $P$ is pressure, $\mu$ is the molecular viscosity, $S_i$ a component of the body forces (includes source terms accounting for forces cause by interaction of the fluid with the fuel spray), $\delta_{ij}$ is the Kronecker delta, $\bar{f}$ is the mean mixture fraction, $S_{m,i}$ is the mass transfer from liquid fuel droplets to gas phase, $\bar{H}$ is the mean total enthalpy, $k_{eff}$ is the effective conductivity, $C_p$ is the specific heat capacity of the fluid, $S_h$ is the source term accounting for any further heat losses, $\bar{f}'2$ is the mixture fraction variance, $\mu_t$ is the turbulent viscosity, $\sigma$ is the laminar Prandtl number, $\sigma_t$ is the turbulent Prandtl number, $k$ is the turbulent kinetic energy, $\varepsilon$ is the energy dissipation rate. $C_g$ and $C_d$ are constants. The mixture fraction is given by $f = (Z_l - Z_{l,ox})/(Z_{l,fuel} - Z_{l,ox})$,where $Z_l$ is the elemental mass fraction for an element $l$, the subscript $ox$ denotes the mass fraction at the oxidiser stream inlet and the subscript *fuel* denotes the mass fraction at the fuel stream inlet, $D$ is the effective diffusion coefficient, $S_{NO}$ is the components of sources in the gas phase, $\sigma_{soot}$ is the turbulent Prandtl number for soot transport and $R_{soot}$ is a component of the net rate of soot generation. The source term of the $NO_x$ transport equation, $S_{NO}$ is calculated with respect to thermal and prompt $NO$ mechanisms. The source term of the soot transport equation, $R_{soot}$ is calculated using an empirical rate expression.

In this study the standard $k-\varepsilon$ turbulence model with standard wall functions is used to close the URANS equations. The eddy viscosity term is modelled using the equation, $\mu_t = \rho C_\mu k^2/\varepsilon$, where $C_\mu$ is a constant. The non-adiabatic non-premixed combustion model is employed, where the enthalpy defect experienced at the vicinity of the wall is included in the flamelet generation. The diesel unsteady laminar flamelet combustion model is used to describe thermo-chemical coupling by solving one-dimensional unsteady flamelet equations for a laminar counter-flow configuration [34]. An assumed beta probability density function ($\beta$-PDF) is used to link turbulence and chemistry. The diesel fuel chemistry is represented by an n-heptane mechanism consisting of 29 species and 52 reactions [35] and is supplemented with a $NO_x$ submehcanism consisting of 4 species and 12 reactions [36], both of which are validated for engine relevant conditions. The liquid fuel injection is handled as a discrete phase which evaporates and then mixes with air in the chamber. Droplet diameters are assumed to be uniform and injection is controlled by mass flow rate profiles (see Fig. 4 a)) containing pilot and main injections. An injector hole diameter of 0.15 mm and included spray angle of 140 deg are used. The discrete phase model analytically tracks injection droplets with the fluid flow time step and models their interaction with the continuous phase using stochastic collisions and breakup models. Table 1 gives a summary of the numerical models used to account for turbulence, combustion, fuel spray, pollutants and the dynamic mesh.

A 3-D double precision analysis is carried out using the pressure

**Table 1**
Numerical models used in this investigation.

| Description | Model |
|---|---|
| Viscous | $k-\varepsilon$ |
| Energy/Species | Non-adiabatic non-premixed combustion |
| | Diesel unsteady flamelet model |
| | Chemkin mechanism and thermodynamic database |
| Discrete Phase | Droplet particle |
| | KHRT breakup |
| | Stochastic collision |
| | Wall-film boundary condition |
| $NO_x$ | Thermal |
| | Prompt |
| Soot | One-step |
| Dynamic mesh | Layering and Smoothing |

based solver to compute the solution. Pressure-velocity coupling algorithms are used to derive an additional condition for pressure by reformatting the continuity equation and obtaining a pressure field. PISO scheme is used due to its suitability for transient flows in terms of achieving faster convergence and lower computational cost. Second order upwind schemes are used for the spatial discretisation. Least squares cell-based method is used to compute gradients. First-order implicit time-stepping is used due to the variable time step profile which is used to refine time-steps at injection and throughout the main combustion phase. Convergence criteria are set to converge at residuals of $10^{-3}$ apart from energy which is set to $10^{-6}$. Max iterations per time step are set to 50. Convergence criteria for the post-processed $NO_x$ and soot scalars are set to $10^{-6}$ with a maximum number of post-iterations each time step of 10. Table 2 outlines a summary of numerical methods employed for the calculation.

### 2.2. Numerical setup and validation

Experimental data from a four-stroke turbocharged diesel direct injection CI engine from Tsujimura et al. [31] was used to validate the simulations using data for engine geometry, in-cylinder pressure, heat release rate, injected fuel mass and injection timings. This engine specification shares a number of similarities with the prototype CVCP engine described in section 1. Table 3 provides engine specifications for the reference engine at high and low load conditions.

A 51.43 deg geometry representing 1/7th of the full combustion chamber was created with SOLIDWORKS and then meshed using Ansys Workbench (Fig. 3.). Meshing a sector allows for a large reduction in computational costs and is possible due to the symmetry of the 7 injector holes in the combustion chamber. The mesh is refined in the piston bowl region and inflation layers are added to the piston walls. A mostly hex mesh is used to reduce numerical diffusion and increase computational efficiency. Due to movement of the piston, a rigid dynamic mesh is used to model compression and power strokes. The dynamic mesh model allows for the boundaries of cell zones to move relative to other boundaries of the zone. A smoothing and layering method is utilised in this analysis.

Constant temperature boundary conditions (which assume the engine has already been run for a number of cycles) are applied to deal with heat transfer at the gas–solid boundaries, temperatures are provided in Table 4. Using the constant temperature condition means that the wall need not be meshed and is a reasonable assumption due to the relatively small time scales. No slip boundary conditions are also applied at the solid walls. The discrete phase model uses a wall film condition at the solid boundaries, which is described by the stanton-rutland impingement/splashing model. Periodic boundary conditions are specified along the side faces of the sector to simulate a full engine.

EGR is implemented by replacing a percentage of the intake air with exhaust gases. This is achieved by changing the oxidiser stream composition in the flamelet and a form of cooled EGR is assumed so initial temperature is unchanged. Relations for the exhaust gas stream composition are deduced from [24]:

$$CH_y + \left(1 + \frac{y}{4}\right)(O_2 + 3.773N_2) \rightarrow CO_2 + \frac{y}{2}H_2O + 3.773\left(1 + \frac{y}{4}\right)N_2, \quad (8)$$

where y is the ratio of hydrogen to carbon in the fuel.

### 2.3. Validation and mesh sensitivity analysis

Results using 3 different mesh resolutions were compared with experimental data in order to select a mesh for the study. Mesh densities were varied by changing minimum element size and maximum face size to ensure the solution is mesh independent and accurate. Table 5 details the number of elements in each mesh at BDC.

Fig. 4 a) shows the comparison of pressure and heat release rate (HRR) between the experimental reference [31] and three mesh densities. Each mesh does a reasonable job at capturing the pressure and HRR profiles, with pre-combustion pressure, igniton delay and initial heat release rate all being represented accurately. The coarse mesh underpredicts peak HRR and combustion pressure at low load and is discarded. Medium and fine meshes do a better job at capturing HRR but still slightly underpredict at both loads while peak combustion pressure is also somewhat overpredicted. Both meshes capture trends well, with the fine mesh showing only minor improvements over the medium mesh. Results are deemed adequately mesh independent and the medium mesh was used during the remainder of the simulations due to reduced computational cost.

Fig. 4 b) compares the emissions predictions obtained using medium mesh at EVO in the simulations with those of the exhaust gases in the reference engine [31]. Soot, $NO_x$ and $CO_2$ trends between low and high load are represented well with all increasing as load increases. Values are somewhat underpredicted however, which can partly be attributed to scaling the results with gross indicated work output and taking values at EVO rather than from exhaust gases due to limitations of the simulations. Discrepancies arise in the UHC plot. It is much more difficult to capture accurate UHC values due to the many intermediate combustion products involved as noted by Kim et al. [37] and a more detailed reaction mechanism is likely required. The earlier heat release of the low load main diesel injection observed in the simulations is another contributing factor as well as the use of n-heptane as a surrogate for diesel. Consideration of the likes of UHCs in the initial compostion of gases at IVC may also be required to reproduce the experimental results more accurately.

**Table 2**
Summary of numerical methods employed for the calculation.

| Description | Parameter | Method/Model/Value |
|---|---|---|
| Solver | General | Pressure-based |
| Pressure-velocity coupling | Flux type | Rhie-Chow |
| | Scheme | PISO |
| | Skewness correction | 1 |
| | Neighbour correction | 1 |
| Spatial discretisation | Gradient | Least square cell based |
| | Density | Second order upwind |
| | Momentum | Second order upwind |
| | Energy | Second order upwind |
| | $k$ | Second order upwind |
| | $\varepsilon$ | Second order upwind |
| | Mean mixture fraction | Second order upwind |
| | Mixture fraction variance | Second order upwind |
| | Pollutant $NO_x$ | Second order upwind |
| | Pollutant soot | Second order upwind |
| Temporal discretisation | Time | First order implicit |

**Table 3**
Engine specifications for the experimental reference engine at high and low load [31].

| Description | High Load | Low Load |
|---|---|---|
| Bore (mm) | 115 | 115 |
| Stroke (mm) | 125 | 125 |
| Compression ratio | 17.5 | 17.5 |
| Initial absolute pressure (bar) | 1.6 | 1.1 |
| Injector holes in full cylinder | 7 | 7 |
| Engine speed (RPM) | 1500 | 1500 |
| Pilot Signal Start of Injection (CA) | 710.1 | 713.1 |
| Pilot Diesel Injection Volume ($mm^3$) | 1.2 | 1.0 |
| Main Signal Start of Injection (CA) | 726.1 | 724.1 |
| Main Diesel Injection Volume ($mm^3$) | 76 | 22 |
| Total fuel energy (J) | 2756 | 821 |
| IMEP (MPa) | 0.9 | 0.3 |

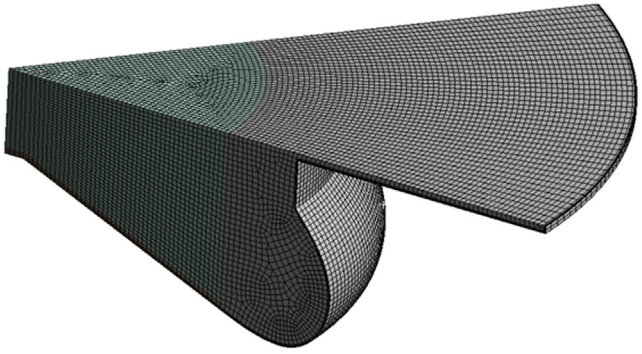

**Fig. 3.** Medium density mesh at TDC.

## 3. Results and discussion

In this work the effect of start time and duration of CVCP at low and high loads is investigated. Simulations of both conventional and CVCP cycles are carried out and combustion characteristics, efficiency and emissions are compared. Section 3.1 focuses on the effects of CVCP start time. Section 3.2 investigates the effects of CVCP duration. Section 3.3 examines further emission reduction strategies.

Fig. 5(a) shows the schematic of the conventional “Base” test cases where fuel injection occurs when the piston is near TDC and then combustion with normal reciprocating motion, while Fig. 5(b) shows the schematic of CVCP test cases where fuel injection and combustion occur at TDC. Fig. 6 shows an example of the piston profiles used in the test cases. In this investigation 720 crank angle (CA) refers to TDC at the end of the compression stroke in a 4-stroke CI engine.

### 3.1. Varying CVCP start time

The start time of the CVCP in a cycle can have an impact on performance and emissions. To evaluate the effect of CVCP start time, three different CVCP start crank angles are tested, namely: 40cv700, 40cv710 and 40cv720 which refer to cases with a CVCP duration of 40 deg and start times of 700CA, 710CA and 720CA respectively. These are then compared with the conventional engine results denoted as Base. Table 6 details the test cases.

#### 3.1.1. Combustion characteristics

Fig. 7 shows the in-cylinder pressure and HRR curves at high load for the 3 CVCP cases and the conventional Base case. All cases show an initial ignition delay phase of roughly 1CA with little to no difference between any of the cases due to temperature and pressure being largely the same at start of injection in all cases. All cases also show similar premixed-charge combustion phases due to the time for mixing being almost identical between cases, there is however a faster fall off from peak HRR in CVCP cases. The early increase in heat release is expected due to the higher pressures and temperatures leading to improved combustion. The faster fall off in HRR is due both to there being less fuel/oxidiser availability as more has been burned and the reduced piston motion leading to poorer mixing of newly injected fuel and oxidiser compared to the conventional engine. The major difference in HRR between CVCP and conventional cases appears during the non-premixed combustion phase, where a secondary peak in HRR occurs. This secondary peak is the result of increased temperature and pressure allowing for a higher quantity of the fuel to combust due to much higher likelihood that the mixture is within its flammability limits. There is also another uptick in HRR in the CVCP cases which is not present in the conventional case when the piston begins to move after being held at TDC. This is due to the displacement of fuel which has not had a chance to mix properly with oxidiser, a mechanism which is also somewhat enhanced by the faster piston acceleration away from TDC, evidenced by the HRR being highest at this point in 40cv720 i.e. the case with the fastest piston movement after TDC. This is then followed by the late combustion phase where minimal amounts of combustion occur with the conventional engine showing slightly higher amounts of HRR as the piston approaches EVO due to there being slightly more unburned fuel remaining in the cylinder. It should be noted that 40cv700 has the fastest approach to TDC with 40cv710 being slower and 40cv720 slower still (same as conventional) while the opposite is true for movement away from TDC after the CVCP.

The main combustion event in the conventional engine occurs sometime after TDC due to the engines operation not being fully optimised with regards to pure diesel operation and performance [31,38] which is a factor in the reduced levels of HRR. Peak pressure in the conventional engine is observed to be 7.32 MPa while as expected the CVCP cases show much higher peak pressures of around 15.3 MPa. The higher pressures are the results of piston being held at TDC and therefore all of the combustion energy is built up until the CVCP ends and the piston is released. Higher pressures are then observed for the majority of the expansion stroke until around 50 deg after each CVCP ends. There is very little difference between pressure rise rate, peak pressure and HRR when comparing the 3 CVCP cases. The only major differences between the 3 cases is the offsetting of each pistons approach to TDC causing pressure to rise prior to the conventional TDC in the two early start times, fuel injection and therefore combustion being offset from one another successively by 10 degrees and the slightly faster piston acceleration away from TDC the later the CVCP ends.

One of the issues that these graphs highlight is two instances of a long dwell time at TDC in all CVCP cases. First is the time between pilot and main injections being too spaced out. This leads to the pressure being largely stagnant for the first 20CA of the CVCPs-either the pilot should be removed, and the main injection substituted in its place or the dwell time between pilot and main injection should be reduced. Utilising the full CVCP is important as work is not generated until the expansion begins and if expansion could start for example 20CA earlier work output would also increase. The second instance of long dwell time is the levelling off in pressure rise rate observed towards the latter stages of the non-premixed combustion phases. It could be more beneficial to end the CVCP earlier when the pressure rise rate begins to reduce as this would not impact performance too greatly, and could lead to an increase if the increased expansion stroke increases work more than the further combustion would. This approach would likely lower $NO_x$ significantly due to high temperatures being maintained for a shorter time period. While not investigated in this study, it should also be noted that RPM will alter how much of the CVCP is fully utilised. At lower RPMs long dwell time would increase and at higher RPMs reduce as actual time spent at TDC changes while rate of combustion generally does not. This long dwell time is beneficial at higher engine speeds when the time spent at TDC is shorter.

Fig. 8 shows average in-cylinder temperatures for each case.

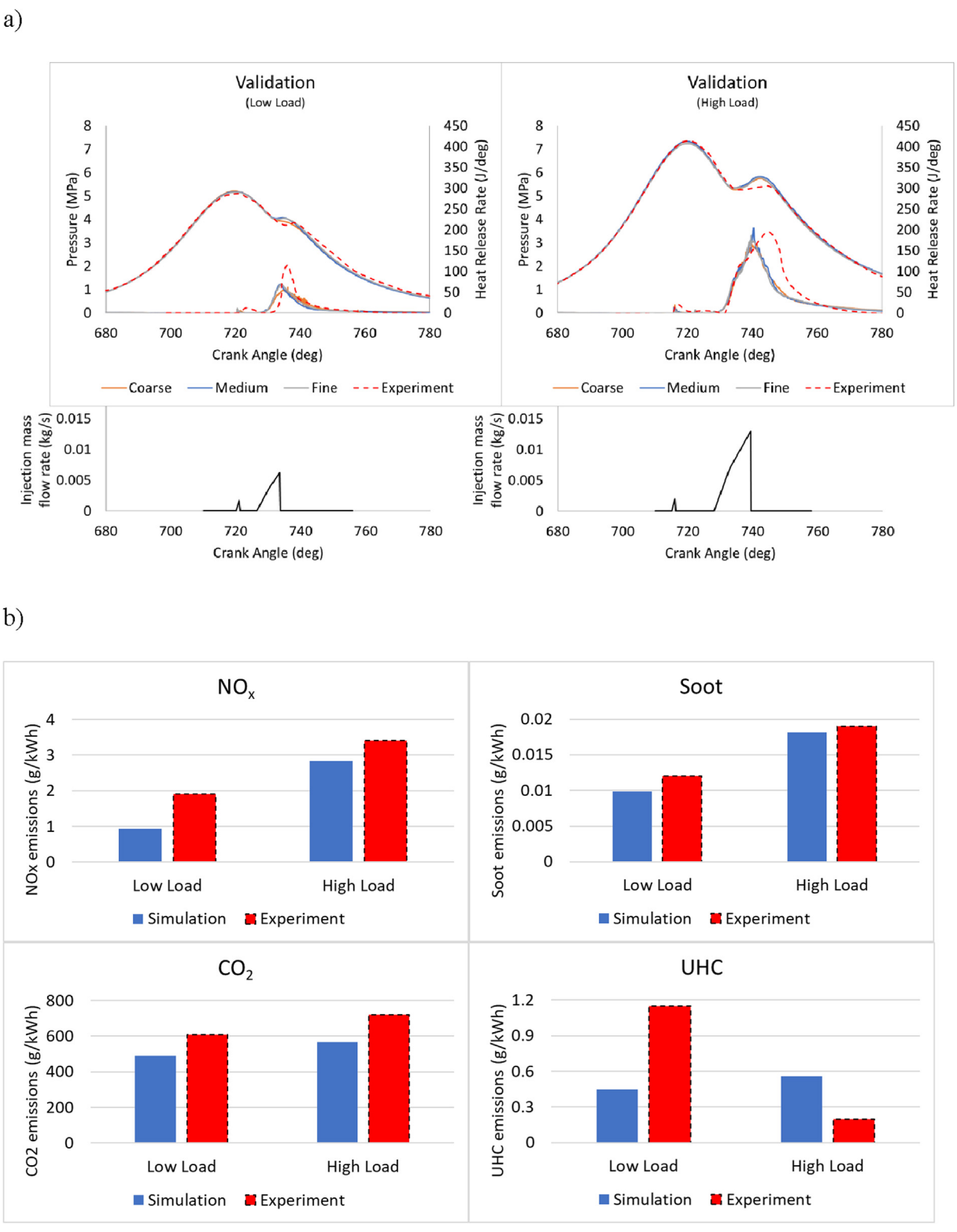


**Fig. 4.** Validation for the high and low load simulations against the experimental reference [31] for a) pressure and heat release rate and fuel injection mass flow rate profiles, b) soot, $NO_x$, $CO_2$ and UHC emissions.

Average in-cylinder temperatures are for the most part higher for all CVCP cases when compared to the conventional case, with the conventional case only having slightly higher temperature during the late power stroke. Average in-cylinder temperatures in the CVCP cases increase until the end of the CVCP due to the build-up of pressure and heat released by the combustion, but fall off more rapidly once the piston begins to move again, whereas the conventional case peaks during fuel injection and temperatures fall off more steadily. The rapid fall off in temperature is due to higher amounts of heat loss to the walls, faster piston movement away from TDC and reduced amounts of excess fuel/oxidiser left for combustion when compared to the conventional case. Peak in-cylinder temperatures are about 50 K higher in the CVCP

**Table 4**
Constant temperature boundary conditions.

| Zone | Temperature (K) |
|---|---|
| Chamber main liner face | 500 |
| Chamber top liner face | |
| Piston liner face | |
| Chamber top face | 600 |
| Piston bottom face | 650 |

**Table 5**
Mesh densities for validation and mesh sensitivity anaylsis.

| Mesh Density | Elements |
|---|---|
| Coarse | 443,868 |
| Medium | 746,063 |
| Fine | 1,177,867 |

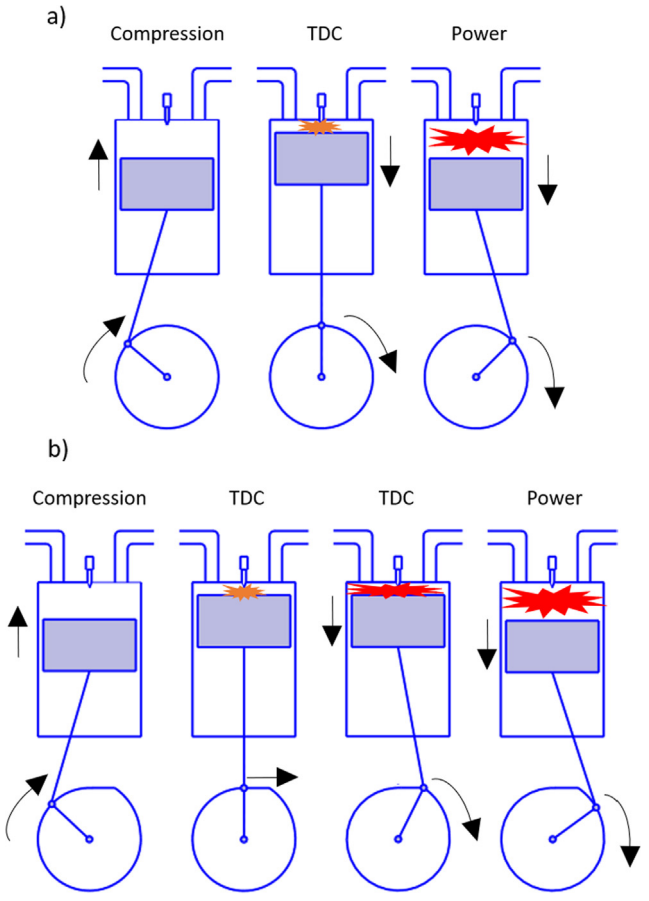


**Fig. 5.** (a) Schematic of the conventional Base test case, (b) Schematic of CVCP test cases.

cases compared to the Base case (roughly 2720 k vs. 2670 K). Similar maximum temperatures are reached during/just after the main fuel injection in the CVCP cases due to the build-up of energy but lower maximum temperatures are observed in the conventional engine due to the lower pressure, chamber expansion and reduced amounts of pre-mixed combustion. Comparing the CVCP cases, temperatures are generally higher for longer when earlier CVCP start times are used, owing to fuel injection and therefore combustion occurring earlier. This is somewhat counteracted by the faster piston movement in the later CVCP start times but average in-cylinder temperatures at EVO are essentially equal and roughly 150 K lower than that of the conventional

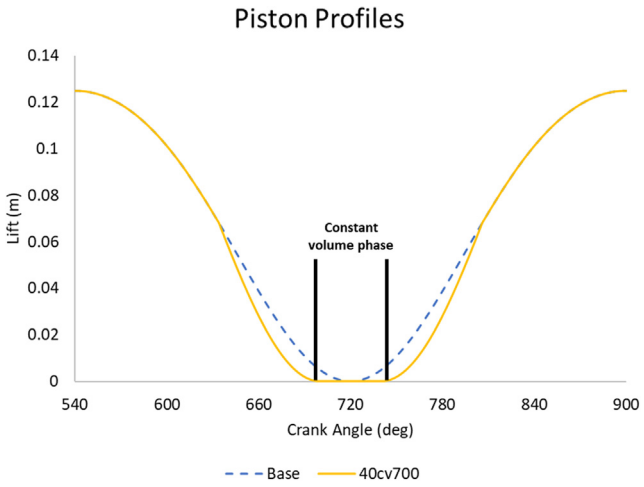


**Fig. 6.** Example piston profiles used in Base and 40cv700 test cases.

**Table 6**
CVCP start time test cases. All at high load with 40 deg CVCP duration.

| Description | Base | 40cv700 | 40cv710 | 40cv720 |
|---|---|---|---|---|
| CVCP period (CA) | – | 700–740 | 710–750 | 720–760 |
| Injection period (CA) | 714–739 | 700–725 | 710–735 | 720–745 |

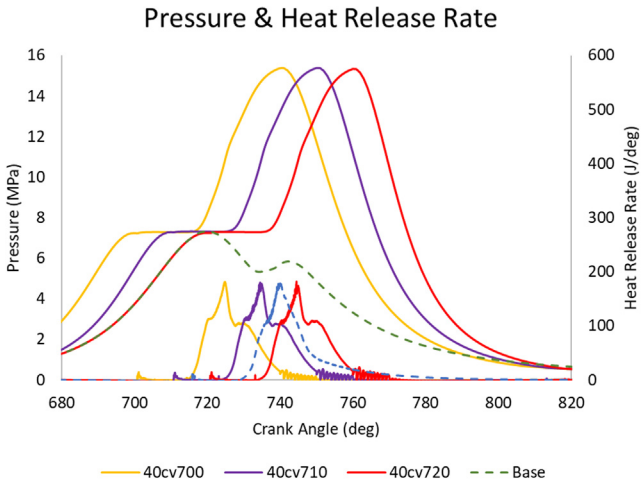


**Fig. 7.** Pressure and HRR-CVCP start time.

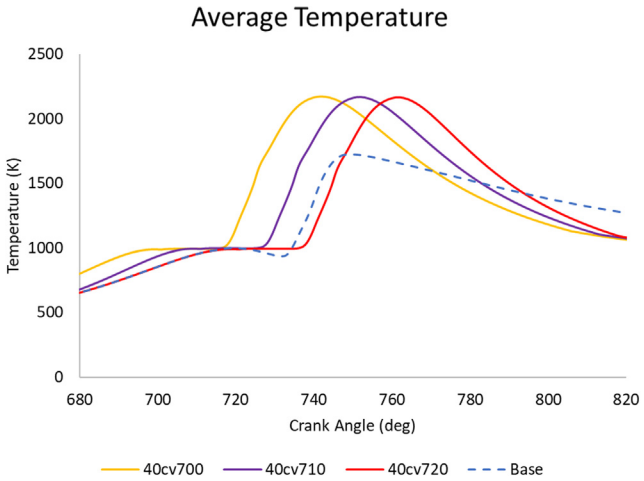


**Fig. 8.** Average temperature-CVCP start time.

engine.

### 3.1.2. Emissions

UHC emissions are a good indicator for the quality of combustion which occurred as the lower the value the more complete the combustion and the more fuel which was utilised. A number of factors can cause high UHC emissions including poor mixing of fuel and oxidiser, low temperatures, fuel getting caught in small crevices and fuel mixing with lubricating oil [39]. Fig. 9(a) shows UHC emissions reduce dramatically with implementation of the CVCP indicating a much more efficient conversion of fuel to work. This is a result of large amounts of complete combustion occurring at a constant volume and the higher temperatures and pressures being ideal for high combustion efficiencies. The reduced mixing caused by the stationary piston is clearly outweighed by the improved thermodynamic conditions. The 40cv720 case shows the highest UHC values out of the 3 CVCP cases which is likely due to the shorter amount of time allowed for slower reactions to occur before EVO and slightly reduced mixing due to the slower compression stroke. This is an important finding: that CVC can give significantly reduced UHC emissions, indicative of significantly more efficient conversion of fuel into work; i.e. appreciably higher efficiency meaning lower fuel consumption.

Soot emissions are sensitive to many factors, with the main cause of high soot production being areas of locally rich carbon and low temperatures [40]. Fig. 9(b) shows the CVCP cases produce low soot levels which are an order of magnitude smaller than the conventional setup. The low soot levels in the CVCP cases are due to the higher temperatures and high levels of combustion efficiency during the CVCP leading to very few rich distributions of carbon in the cylinder, as a large quantity of the injected fuel has gone through quality, complete, combustion. Fast movement of the piston after the CVCP ends also promotes the oxidisation of soot and thus reduces its formation further. Again, the highest soot levels out of all CVCP cases is that of the late CVCP start time and is likely the result of the increased UHC levels leading to some locally rich carbon distributions where soot can form and faster fall off in temperature due to the shortened expansion.

$NO_x$ emission is sensitive to in-cylinder temperatures due to the thermal Zeldovich mechanism [41] with thermal $NO_x$ production rate doubling with every 90 K increase above 2200 K but falling to much lower rates when temperatures are below 1800 K [42]. As expected, the prolonged higher temperatures associated with the CVCP strategy lead to a significant increase in $NO_x$ emission, as shown in Fig. 9(c). $NO_x$ emissions are shown to be 6 times higher than the conventional case and are therefore clearly one of the limiting factors when implementing a CVCP cycle and optimisation is required to reduce their level. The later CVCP starts lead to a small reduction in $NO_x$ due to the faster temperature fall off and fuel injection closer to EVO.

Similar to UHC, high levels of $CO_2$ are generally an indicator that the fuel has undergone complete combustion as a larger quantity of CO in the chamber has been oxidised. While this trend is followed on a per cycle basis in this analysis i.e. CVCP cases tend to have higher $CO_2$ levels than the conventional case on a cycle by cycle basis, Fig. 9 (d) however shows that the specific output of $CO_2$ is highest in the conventional case. This is down to the increase in performance/efficiency attributed to the CVCP outweighing the increased $CO_2$ per cycle in those cases when compared to the conventional case.

### 3.1.3. Performance

Gross indicated performance characteristics are calculated and any further mention of performance refers to gross indicated performance. Trapezoidal rule [43] is used to integrate and find the area between P-V curves for each case, providing the work and from this power, indicated mean effective pressure (IMEP) and thermal efficiency were calculated. All performance characteristics are linearly linked and therefore only thermal efficiency is presented in Fig. 10.

The CVCP leads to increases to thermal efficiencies by 7–8%

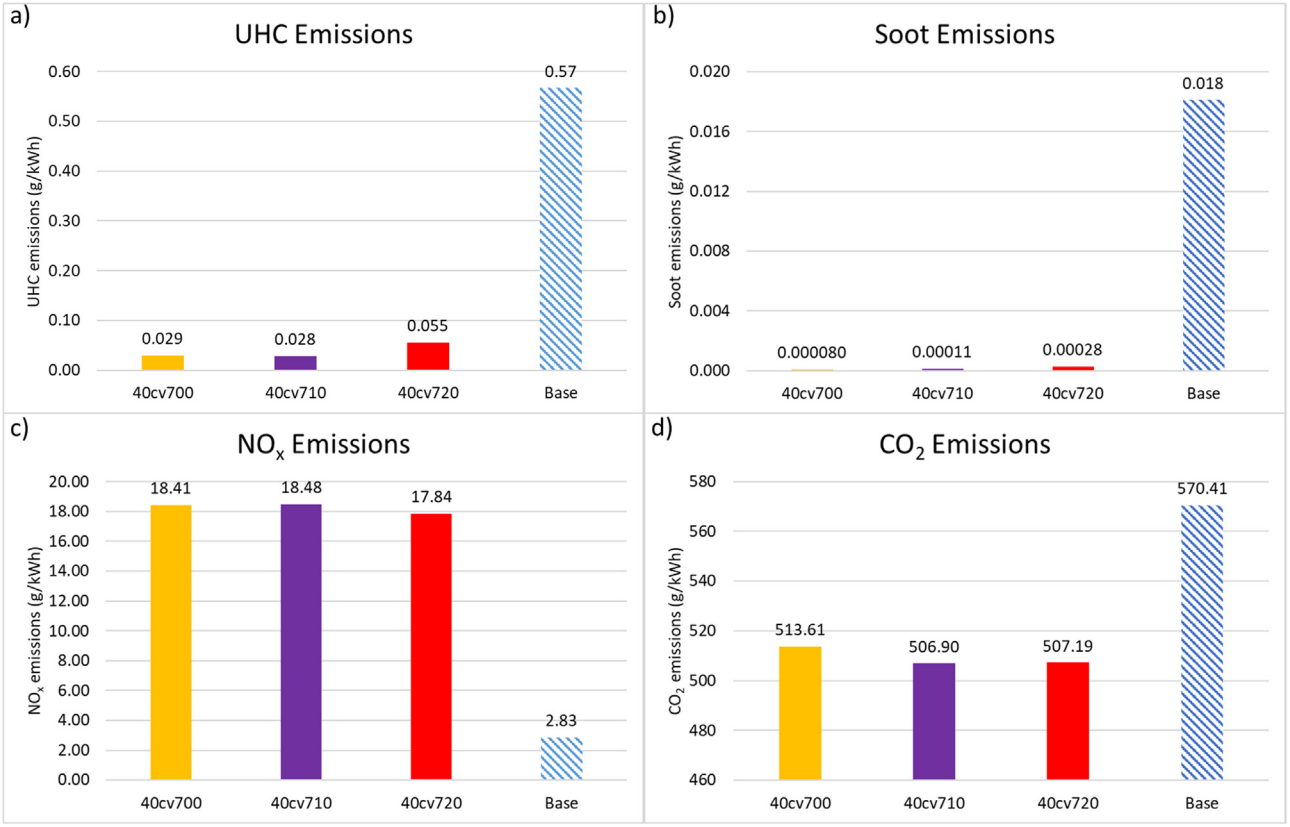


**Fig. 9.** Emissions levels at EVO for (a) UHC, (b) Soot and (c) NOx and (d) $CO_2$-CVCP start time.

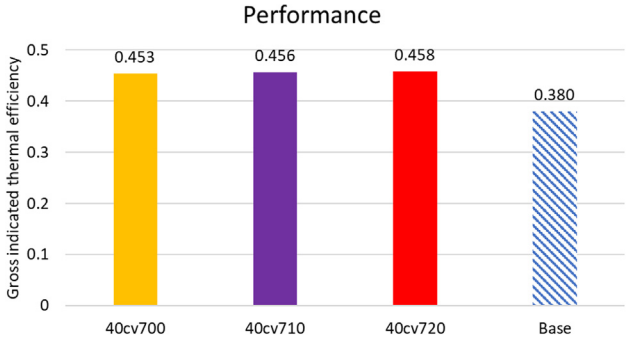


**Fig. 10.** Performance characteristics for thermal efficiency-CVCP start time.

compared to the conventional engine-a reduction of specific fuel consumption (SFC) by over 20%. The increase in performance is caused by factors including: increased fuel utilisation, higher in-cylinder pressures and temperatures being built to drive the piston and increased amounts of combustion occurring at these conditions. The reduced expansion stroke caused by later CVCP start times appears to be largely balanced out by the longer compression stroke and increased piston speed when moving away from TDC enhancing mixing and therefore promoting combustion, leading to very similar thermal efficiencies between the CVCP cases.

There is room for improvement in terms of performance increases due to the previously mentioned long dwell time during the CVCP phases. This can be achieved through injection profile optimisation and or reduction of the CVCP duration to eliminate the constant pressure region and fall off in pressure rise rate. The following two sections explore these options.

### 3.2. Varying CVCP duration

Three different CVCP durations are tested, namely: 20 deg (CV20), 30 deg (CV30) and 40 deg (CV40) and are compared to the conventional "Base2" test case. In all cases dwell time between pilot and main injection has been reduced to address the long dwell time at TDC discussed in the previous section. All CVCP start at 720CA to allow for easier comparison to the conventional test case and low load cases are introduced to gauge the effectiveness of the CVCP cycle across multiple engine loads. Table 7 outlines the cases.

#### 3.2.1. Combustion characteristics

Fig. 11 shows the in-cylinder pressure and HRR for the 3 CVCP durations and conventional engine test cases at low and high loads. All cases at a given load condition show very similar ignition delay timings with no considerable differences between each other. High load cases exhibit the same trends as the previous section with slightly increased initial HRR, faster fall off from peak, secondary peak and uptick upon piston release. HRR at low load shows a large increase in premixed-charge HRR for CVCP operation, but no secondary peak due to the reduced injection volume. Larger amounts of somewhat uneven combustion continue through the CVCPs and HRR also exhibits the upticks when the piston is released from TDC. The upticks are larger however as the quality of combustion is lower in the low load cases when compared to the high load due to the reduced temperatures, pressures and injection velocities meaning there is a high quantity of unburned hydrocarbons available for combustion at the end of each CVCP.

At high load peak pressure in the conventional engine is observed to be 7.25 MPa while the CVCP cases show peak pressures of 12.15 MPa, 14.86 MPa and 15.51 MPa for CV20, CV30 and CV40 respectively. At low load peak pressure in the conventional engine is observed to be 5.18 MPa, while CV20, CV30 and CV40 have peak pressures of 6.92 MPa, 7.37 MPa and 7.52 MPa respectively. The higher pressures are the result of much of the combustion occurring at a constant volume while the piston is being held at TDC and the reduction in pressure as CVCP duration decreases is simply due to there being less time for pressure to build and more fuel still needing to undergo complete combustion. Higher pressures are then observed for much of the expansion strokes until around 50 deg after each CVCP ends.

The long dwell time at TDC is still present in all cases with the dwell time between pilot and main injection not being adequately reduced (difficult to reduce further while still comparing fairly to the conventional engine). However, at high load and low load the CV20 cases adequately eliminate the part of the CVCP where pressure rise rate begins to fall off. As do the CV30 cases to a lesser extent but there is still a reduction in pressure rise rate especially at low load where the drop off is far more apparent and will impact engine performance. The lower duration CVCP cases should also benefit from having longer expansion strokes, and therefore time to output work, which will alleviate the loss of potential quality combustion and increased peak pressure which a longer CVCP would have given.

Fig. 12 shows the average in-cylinder temperature at high and low loads. Average temperatures show similar trends across both load conditions. Higher temperatures over a prolonged duration are observed in the longer CVCP test cases due to there being more time for pressure and temperature to build and be maintained. Once released from TDC each CVCP case falls off more quickly than the conventional cases with the rate of fall off increasing the longer the piston was held at TDC due to increased heat transfer to the walls, lesser amounts of fuel being available for combustion and faster piston movement away from TDC. In the late expansion stroke all CVCP cases have lower temperatures than their corresponding conventional case and the longest duration CVCP cases have the lowest temperatures at EVO. Peak temperatures at low load are all within 5 K due to heat transfer counteracting the build-up of temperature once HRR slows down. At high load each successive increase in CVCP duration (0–40 deg) leads to an increase in peak temperature of roughly 30 K.

#### 3.2.2. Emissions

UHC emissions, Fig. 13a), significantly reduce as CVCP duration is increased at both load conditions, but the amount of reduction levels out after CV20. The trends indicate that the longer CVCP duration leads to higher levels of quality complete combustion of the fuel–air mix. The benefits falling off at low load are linked to the reduction in pressure rise rate and therefore performance/specific output. Most of the fuel which could go through complete combustion already has and the remainder is not mixed well with oxidiser and the longer the piston is held at TDC the more likely it is to accumulate.

For similar reasons there is an initial significant reduction in soot between conventional and CV20 but much less of a reduction between

**Table 7**
Simulated test cases for CVCP duration at low and high load. All with CVCP start time of 720CA.

| Case | Base2 | CV20 | CV30 | CV40 | Base2 | CV20 | CV30 | CV40 |
|---|---|---|---|---|---|---|---|---|
| Load | Low | | | | High | | | |
| Constant volume period (CA) | – | 720–740 | 720–750 | 720–760 | – | 720–740 | 720–750 | 720–760 |
| Constant volume duration (deg) | 0 | 20 | 30 | 40 | 0 | 20 | 30 | 40 |
| Injection period (CA) | 720–736 | | | | 720–740 | | | |
| Mass of fuel injected (kg) | 1.93e−5 | | | | 6.49e−5 | | | |

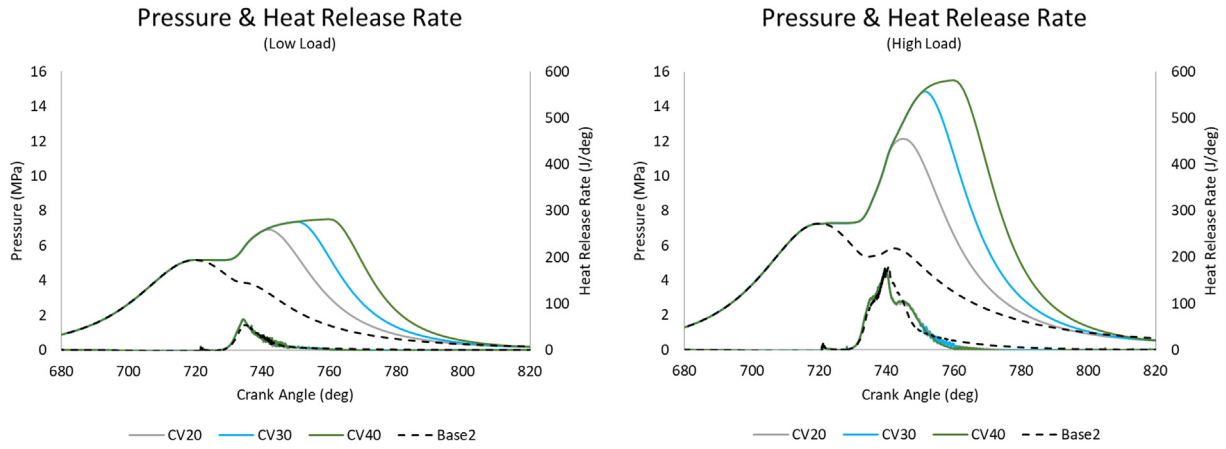


**Fig. 11.** Pressure and HRR at low and high load-CVCP duration.

CV20 and CV40 at both loads, Fig. 13b). The reduced amounts of UHC and higher temperatures greatly contribute to the reduction in soot. The accumulation of UHC which can occur as the piston dwells near TDC may also contribute to the slowdown in soot reduction at longer CVCP durations as this can lead to locally rich high carbon areas in which soot can form. However, the levels of soot observed are still much lower than the conventional case soot levels across all CVCP cases at both loads indicating that even a poorly optimised setup lowers carbon-based emissions considerably. The levelling off is also somewhat due to performance reducing slightly at higher CVCP durations due to reduction in expansion work and therefore specific output is impacted.

Fig. 13c) shows that $NO_x$ emissions increase with increasing CVCP duration at both load conditions due to the higher temperatures present for extended periods as duration increases. However, the increase between the conventional case and CV20 is manageable and further optimisation of fuel injections, CVCP duration and potentially the implementation of EGR or LTC technologies for example could bring this value down further while still maintaining the varied benefits of CVCP operation. When CVCP duration is increased beyond 20 deg significant increases to $NO_x$ are observed and a trade-off between performance, UHC, soot and $NO_x$ emissions will need to be made.

$CO_2$ emissions, Fig. 13d), reduce compared to the conventional case at all CVCP durations and loads but show a small increase between CV30 and CV40. In general, the per cycle $CO_2$ emissions increase for CVCP cases compared to the conventional cases due to the more complete combustion and therefore conversion of fuel to $CO_2$ but the much improved performance leads to a reduction in specific output. Comparing the CVCP cases the reduced performance and increased CO oxidation at the longer durations leads to an increased specific output at CV40 and again we observe the general levelling off in reduction after CV20. As with all other carbon-based emissions $CO_2$ levels are still much lower than the conventional case at all CVCP durations.

### 3.2.3. Performance

Thermal efficiency at high and low load is presented in Fig. 14 and a significant increase of 7–8% is observed between conventional and CVCP cases. As expected due to the long dwell time and reduced expansion stroke there is a considerable levelling off in performance after CV20 with CV40 even reducing compared to CV30. CV20 shows the greatest relative increase due to the reduction in the dwell time at TDC and therefore the elimination of the pressure rise rate falls off which is present at other durations. Pressure rise rate fall off is essentially an indicator for the beginning of diminishing returns for CVCP duration increase in terms of performance. While for the most part there is a greater amount of complete combustion and higher peak pressures occurring at longer CVCP durations the reduction in potential work output by shortening the expansion stroke unnecessarily begins to outweigh the combustion benefits, evidenced by the performance decrease between CV30 and CV40.

### 3.2.4. Contour analysis

Fig. 15 shows contours of UHC at 740CA which represents a crank angle both very close to end of injection and before the end of the CVCP in all cases (contour will be the same in CV20, CV30 and CV40) and therefore highlights the difference between fuel injection in the conventional and CVCP engines. There is clearly a wider distribution of fuel in the conventional case with the fuel spray impinging at the top edge of the piston bowl and causing a flow which pushes the mixture both

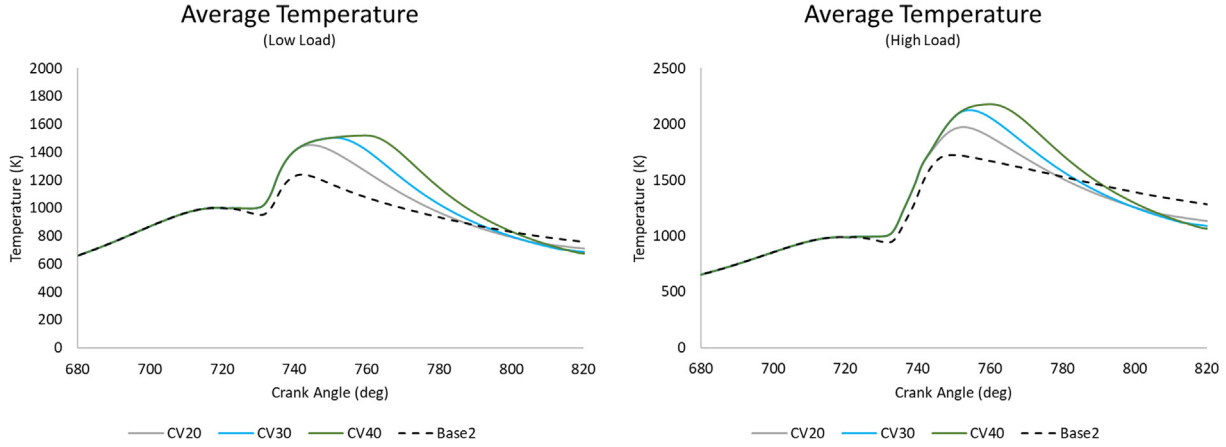


**Fig. 12.** Average temperature at low and high load-CVCP duration.

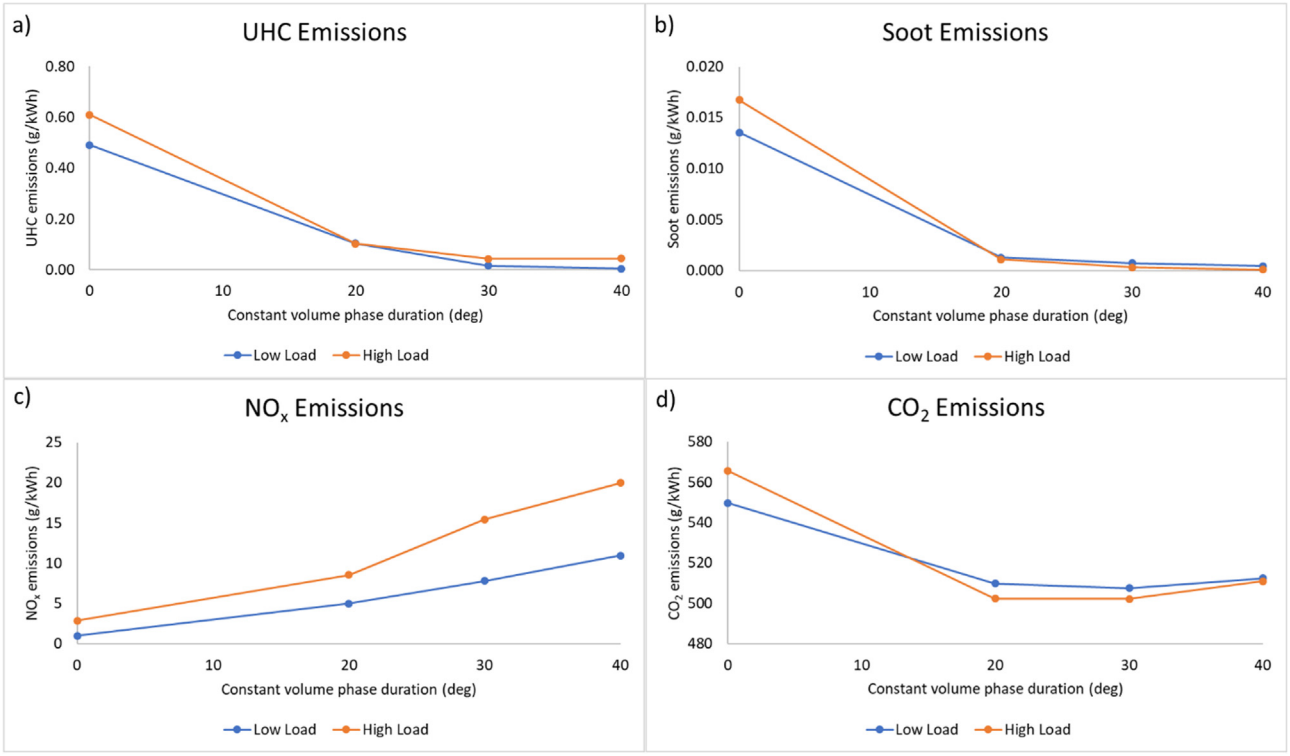


**Fig. 13.** a) UHC, (b) soot, (c) $NO_x$ and (d) $CO_2$ emissions at low and high load-CVCP duration (0 deg represents Base2).

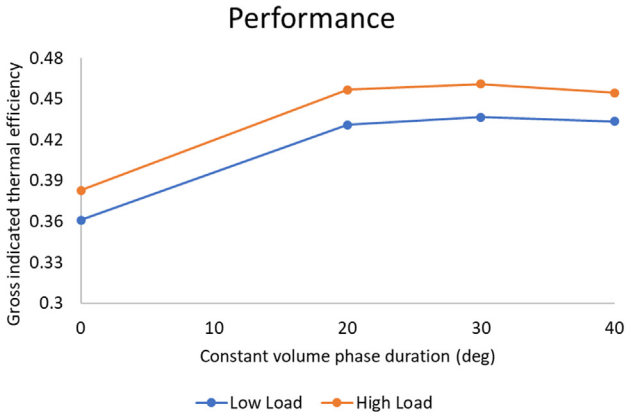


**Fig. 14.** Performance characteristics at low and high load-CVCP duration.

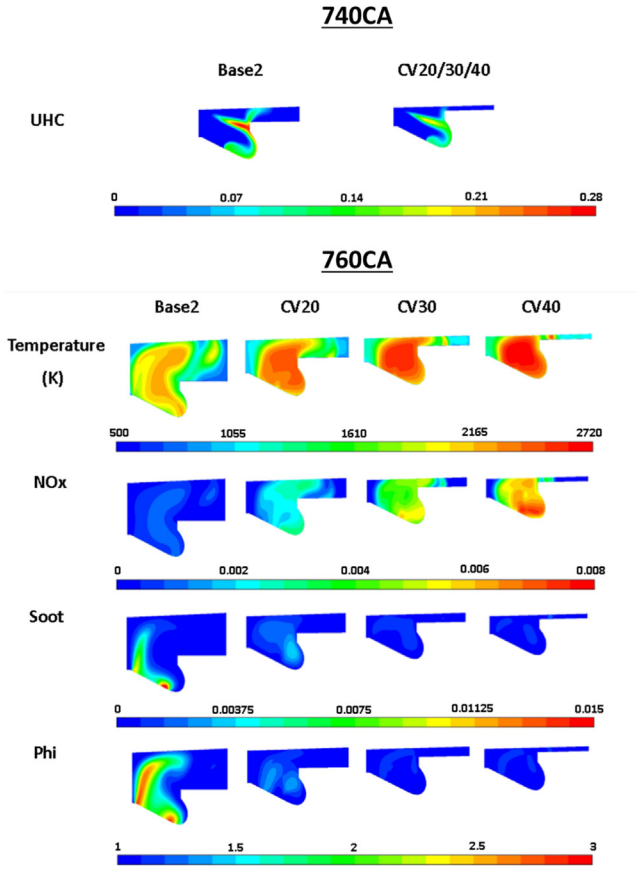


**Fig. 15.** Contours of UHC at 740CA and temperature, $NO_x$, soot and fuel air equivalence ratio at 760CA for the high load cases-CVCP duration.

towards the top face/liner of the cylinder as well as along the piston bowl wall and towards the bowl centre. Whereas in the CVCP cases the fuel spray is incident lower, much more towards the piston bowl, and while a similar pattern emerges in that some of the fuel reflects upwards, the majority moves along the piston bowl wall and towards the centre of the bowl. With that said, even with the reduced level of mixing involved in the CVCP cases, the UHC concentrations are much lower compared to the conventional case due to the improved combustion quality and therefore generally reduced levels of UHC.

Contours of temperature, $NO_x$, soot and fuel–air equivalence ratio are depicted for high load at 760CA in Fig. 15. 760CA is chosen due to it being the end of the longest CVCP phase (CV40). Areas of high $NO_x$ production are shown to occur at areas of high temperature, which correspond to the main combustion sites where the fuel spray was aimed. Temperature contours show that combustion is much more spread and of a lower temperature in the conventional case whereas as CVCP duration increases combustion becomes much more focussed on the centre of the piston bowl and temperature increases. This is clearly

reflected by the increased $NO_x$ levels in these areas. The main areas of initial soot production are near to the injector where temperatures are lower and there is increased mixing in the wake of the injection as well as in the piston bowl on the edge of the main combustion site. These areas of early soot formation correspond to zones of rich fuel–air equivalence ratio. Fuel rich areas are much more focussed around the piston bowl area in the CVCP cases due to this being the area where the injection is directed at TDC (piston does not move during injection in any CVCP case). However even with the areas being the focus of the entire fuel injection they are much leaner than the corresponding conventional case due to the higher quality of combustion leading to far reduced levels of UHCs. The high combustion quality in the CVCP cases means that soot has hardly developed comparative to the conventional case.

### 3.3. $No_x$ reduction study

As noted in the previous sections several improvements can be made to the engine operation which should lead to a reduction in $NO_x$ levels and potentially further improve performance of the CVCP strategy. The two avenues explored in this section are EGR and injection profile optimisation. EGR is introduced as this is an effective method for $NO_x$ reduction which when implemented correctly can have minimal impact on engine performance and other emissions outputs [44]. Three different fuel injection profiles are tested to examine the effects of injection rate and the reduction of the long dwell time at the start of the CVCP periods. Finally, a "best" case is tested which combines the most successful EGR and fuel injection profile cases. Each case in this section utilises a 20 deg CVCP starting at 720CA as this constant volume phase duration receives many of the benefits of the strategy while not increasing $NO_x$ as severely as the longer durations. Table 8 outlines the cases.

#### 3.3.1. EGR

A cooled form of EGR is used which assumes exhaust gas recirculation does not change initial in-cylinder temperatures and intake air is replaced by exhaust gases which are made up of $CO_2$, $H_2O$ and $N_2$. Fig. 16 shows the in-cylinder pressure and HRR for 0%, 15% and 25% EGR rates. Increasing the amount of EGR leads to a reduction in peak pressure by 0.58 MPa and 1.06 MPa for 15% and 25% EGR respectively. Pressure rise rate is also reduced as well as peak and total heat release. This is largely the result of a reduction in oxidiser, but dissociation of $CO_2$ and $H_2O$ during combustion and the higher heat capacity of the exhaust gases causing them to act as a heat sink also contributes to the lowering of both combustion rate and rise in temperature.

Fig. 18 shows emission levels at EVO for each test case. The addition of EGR reduces the in-cylinder temperatures and thus there is a considerable reduction in $NO_x$ for the 15% and even more-so 25% EGR rates. However, increasing the rate of EGR also leads to the increase of UHC, soot and $CO_2$ emissions, Fig. 18a), b), d). For $CO_2$ this is largely due to the recycling of $CO_2$ from the previous cycle. For UHC and soot several factors cause the increase. Oxidiser reduction means the amount of fuel rich zones in which soot formation can occur increases as the overall fuel–air equivalence ratio in the chamber increases and also reduces the amount of soot oxidation that is possible. The reduction also means there is less oxidiser for fuel to undergo complete

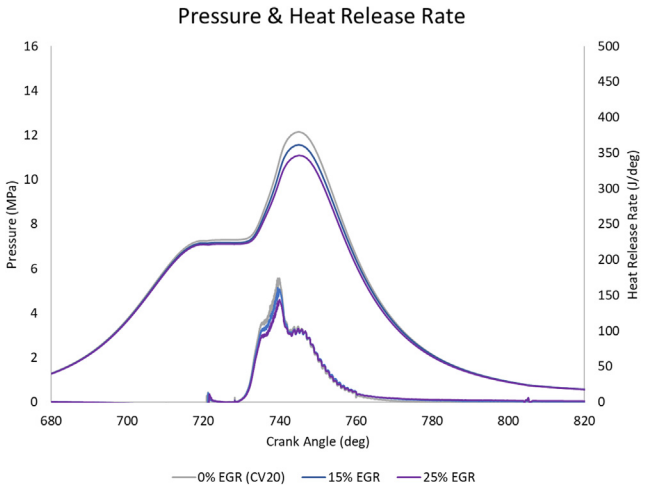


**Fig. 16.** Pressure and HRR for $NO_x$ reduction using EGR.

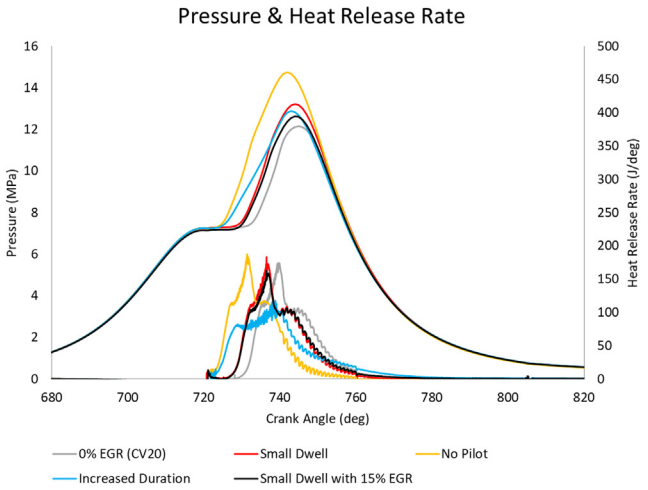


**Fig. 17.** Pressure and HRR for $NO_x$ reduction using varied injection profiles.

combustion with and therefore hydrocarbons are left unburned and more CO is observed due to less oxidation leading to $CO_2$. The increase in UHC also further promotes soot production as there are more locally carbon rich areas. Generally lower in-cylinder temperatures due to the aforementioned dilution, chemical and thermal effects of EGR also promote soot production and UHC increases. Nevertheless, the significant reduction in $NO_x$ when operating under a CVCP strategy is a promising finding.

Fig. 19 shows the thermal efficiencies for each test case. Performance decreases slightly at the low EGR rate but somewhat more significantly at the higher rate. This performance decrease is expected as Fig. 16 shows both pressure at the end of the CVCP period and total heat release are lower as EGR rate increases, thus leading to a lower work output and therefore performance. The finding is also backed up by the increased UHC level, i.e. wasted fuel energy. EGR essentially slows down the rate and total amount of combustion to the benefit of

**Table 8**
Simulated test cases for $NO_x$ reduction. CVCP start time 720CA and duration 20 deg.

| Case | EGR | | | Fuel Injection | | | Best Case |
|---|---|---|---|---|---|---|---|
| | 0% | 15% | 25% | Small Dwell | No Pilot | Increased Duration | Small Dwell + 15% EGR |
| Pilot Injection Period (CA) | 720–722 | | | | – | – | 720–722 |
| Main Injection Period (CA) | 728–739 | | | 725–736 | 720–732 | 720–739 | 725–736 |
| Mass of fuel injected (kg) | 6.49e−5 | | | | | | |

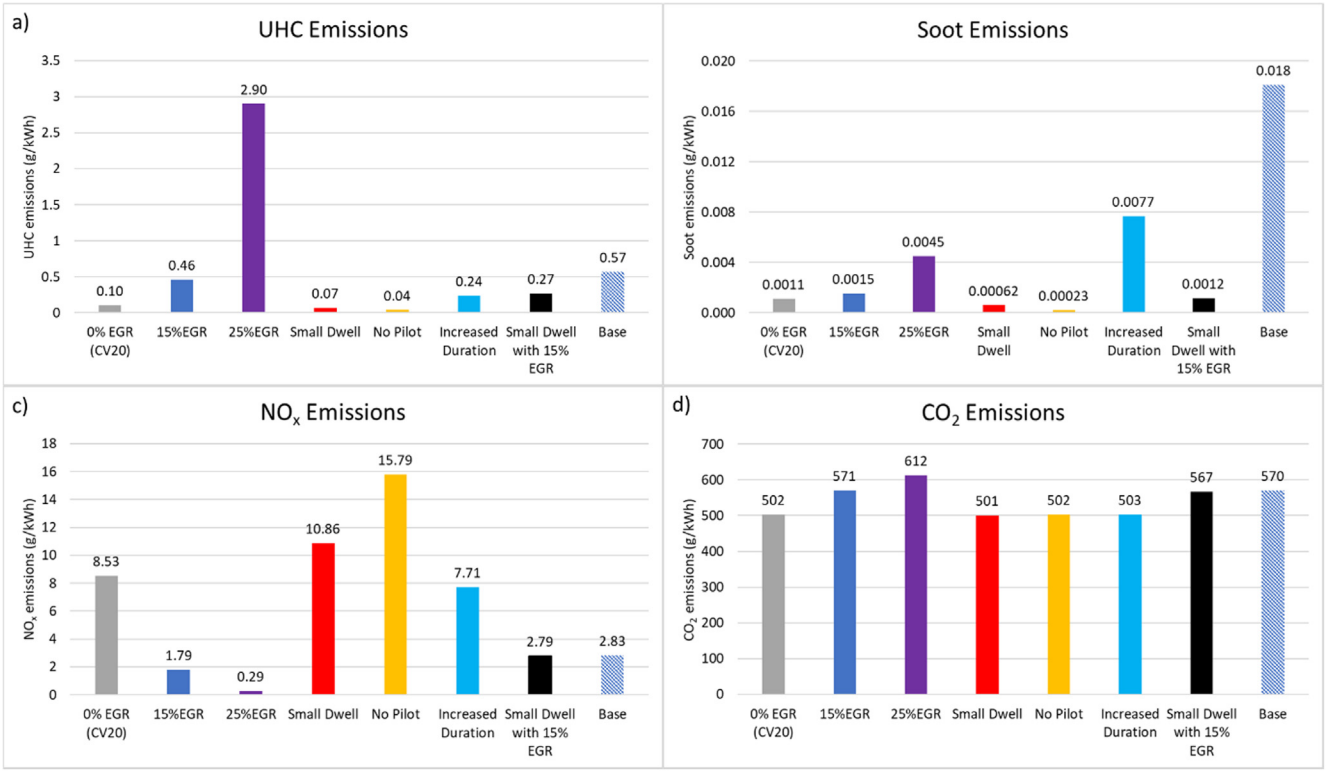


**Fig. 18.** Emissions levels at EVO for (a) UHC, (b) soot and (c) $NO_x$ and d) $CO_2$-$NO_x$ reduction.

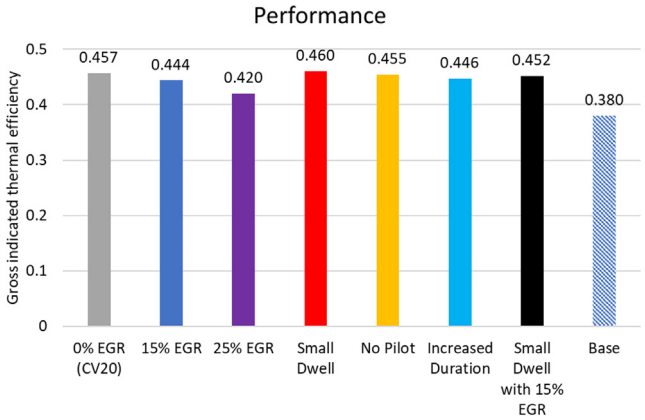


**Fig. 19.** Performance characteristics for thermal efficiency-$NO_x$ reduction.

NOx emissions, but to the determinant of performance, and thus the two must be balanced.

### 3.3.2. Injection profile

The long dwell time at constant volume is addressed by testing 3 new injection profiles. This issue stems from some of the time spent at a constant volume not being used for combustion and therefore either unnecessarily increasing $NO_x$ or and reducing the potential performance gains. The 3 injection profile cases are: Small Dwell which uses a reduced dwell time between pilot and main injection; No Pilot which combines main and pilot injections and moves the main injection to the start of the CVCP phase; and Increased Duration which uses a single long injection with reduced injection rate. Fig. 17 shows the in-cylinder pressure and HRR for the fuel injection profiles.

Clearly No Pilot leads to the greatest increase in peak pressure and has the fastest peak pressure rise rate. This is due to there being a greater amount of time for combustion to occur at a constant volume (fuel injection finishes earliest out of all cases), the increased volume of fuel in the main injection and the increased amount of premixed charge combustion owing to there not being a pilot injection (longer main injection ignition delay). While this does increase performance, Fig. 19, and decrease UHC/soot emissions, Fig. 18a), b), the large increase in $NO_x$, Fig. 18c), due to in-cylinder temperature increases associated with the higher pressures and longer ignition delay likely means this is not a feasible injection strategy.

Increased duration leads to a higher peak pressure than CV20 due to the increased time allowed for fuel to combust at a constant volume. Large amounts of combustion occur in the premixed charge combustion phase due to the lack of pilot injection, but peak pressure rise rate is lower due to the much slower injection rate and slower release of fuel for combustion in the mixing-controlled combustion phase. This injection strategy also has the lowest amount of heat release during the early expansion after the piston is released from TDC which means pressure falls faster and less work is output compared to CV20. Increased fuel injection duration is a reasonable way to maintain $NO_x$ levels while attaining a higher peak pressure due to the temperature rise being slower throughout the CVCP. However, this strategy incurs increases to soot and UHC emissions due to the poorer mixing of the fuel injection leading to zones of high carbon concentrations in the chamber which, when combined with the lower in-cylinder temperatures, leads to UHC and soot formation. Further optimisation of this strategy is required but the pressure increasing while $NO_x$ is maintained means the strategy has potential given better implementation.

Small Dwell achieves the second highest peak pressure while the pilot injection means the peak pressure rise rate is slightly slower than that of the No Pilot test case. The advancement of the main injection allows for a greater amount of combustion to occur in the CVCP when compared to CV20 which in turn leads to the higher pressure, performance and decreased UHC. $NO_x$ does however increase by a small amount due to the increased temperature, a result of the reduced benefit of a pilot with a smaller dwell time between injections. Small Dwell is likely the best of the injection profiles due to the improvements to performance and carbon-based emission outputs, however, none of

the current injection profiles assist adequately with $NO_x$ reduction.

*3.3.3. Combining "Best" EGR and injection profile*

Finally, a combination of the "best" EGR and injection case was carried out to obtain an end result. Small Dwell with 15% EGR was chosen due to the benefits of both strategies outlined previously. Positive results were found with a small peak pressure increase (Fig. 17) observed compared to CV20. The EGR addition reduces the overall combustion rate when compared to the normal Small Dwell case but performance is only slightly reduced. $NO_x$ emissions are much reduced compared to CV20 and even slightly lower than the conventional case. UHC emissions are higher than CV20 but half that of the conventional case while soot emissions climb a small amount but are still much less than in the conventional case. All in all, this strategy would appear to be feasible with $NO_x$ emissions comparable to the conventional engine but much lower soot/UHC emissions and improved performance.

## 4. Conclusions

A comprehensive numerical modelling study has been carried out to assess the benefits of a constant volume combustion phase (CVCP) being implemented in a compression ignition engine with focus on performance/efficiency and emissions. The numerical modelling framework has been validated with experimental data from a conventional turbocharged compression ignition engine. Three-dimensional unsteady Reynolds-averaged Navier-Stokes simulations are performed using a $k-\varepsilon$ turbulence model with diesel unsteady laminar flamelet combustion model being used to describe thermo-chemical coupling.

The study examined the effects of CVCP start time, CVCP duration, EGR addition and injection strategies demonstrating that a properly optimised CVCP engine has many benefits, in terms of pollutant emissions and performance, compared to conventional engine operation.

Key findings and conclusions are as follows:

1. The CVCP strategy was shown to increase thermal efficiency by up to 8%, representing a reduction in specific fuel consumption of up to 20% compared to conventional engine operation.
2. The CVCP strategy leads to a large reduction in carbon-based emissions with soot and UHC values often being an order of magnitude smaller compared to conventional engine operation.
3. The CVCP strategy incurs large increase to $NO_x$ compared to conventional engine operation, however this can be negated by the introduction of low levels of EGR and in combination with the correct injection strategy does not sacrifice the benefits listed above.
4. The CVCP strategy leads to higher peak in-cylinder pressures and temperatures compared to conventional engine operation with greater amounts of heat release during the non-premixed charge combustion phase.
5. CVCP start time has very little impact on emissions and performance allowing for flexibility in engine balancing later in the design process.
6. Increasing CVCP duration beyond a certain point (CV20 in this study) leads to large increases in $NO_x$ emissions and diminishing returns in terms of performance and carbon-based emissions reductions due to pressure rise rate fall-off and dwell time spent at TDC when work output could have begun if the piston was released earlier.
7. EGR rates as low as 15% are shown to greatly reduce $NO_x$ emissions and when combined with improved injection strategies which reduce the amount of dwell time during the CVCP, such as decreasing dwell time between pilot and main diesel injections, can maintain the improvement in performance and reduction in carbon based emissions.

The key findings of the present numerical study on CVCP start time, CVCP duration, EGR addition and diesel fuel injection strategy will be considered in the optimisation of the CVCP opposed piston engine currently being developed by the Covaxe Group [32].

## CRediT authorship contribution statement

**C.J. Ramsay:** Software, Validation. **K.K.J. Ranga Dinesh:** Supervision. **W. Fairney:** . **N. Vaughan:** .

## Declaration of Competing Interest

The authors declare that they have no known competing financial interests or personal relationships that could have appeared to influence the work reported in this paper.

## References

[1] Wallington TJ, Lambert CK, Ruona WC. Diesel vehicles and sustainable mobility in the U.S. Energy Policy 2013;54:47–53. https://doi.org/10.1016/j.enpol.2011.11.068.
[2] Mwangi JK, Lee W-J, Chang Y-C, Chen C-Y, Wang L-C. An overview: energy saving and pollution reduction by using green fuel blends in diesel engines. Appl Energy 2015;159:214–36. https://doi.org/10.1016/j.apenergy.2015.08.084.
[3] Gill SS, Tsolakis A, Herreros JM, York APE. Diesel emissions improvements through the use of biodiesel or oxygenated blending components. Fuel 2012;95:578–86. https://doi.org/10.1016/j.fuel.2011.11.047.
[4] Squaiella LLF, Martins CA, Lacava PT. Strategies for emission control in diesel engine to meet Euro VI. Fuel 2013;104:183–93. https://doi.org/10.1016/j.fuel.2012.07.027.
[5] European Union. COMMISSION REGULATION (EU) No 136/2014 of 11 February 2014. Off J Eur Union 2014. http://data.europa.eu/eli/reg/2014/136/oj.
[6] Pierpont DA, Montgomery DT, Reitz RD. Reducing particulate and NOx using multiple injections and EGR in a D.I. diesel. SAE Trans 1995;104:171–83.
[7] Reitz RD. Directions in internal combustion engine research. Combust Flame 2013;1:1–8. https://doi.org/10.1016/j.combustflame.2012.11.002.
[8] Dec JE. Advanced compression-ignition engines—understanding the in-cylinder processes. Proc Combust Inst 2009;32:2727–42. https://doi.org/10.1016/j.proci.2008.08.008.
[9] Jain A, Singh AP, Agarwal AK. Effect of fuel injection parameters on combustion stability and emissions of a mineral diesel fueled partially premixed charge compression ignition (PCCI) engine. Appl Energy 2017;190:658–69. https://doi.org/10.1016/j.apenergy.2016.12.164.
[10] Li Y, Jia M, Chang Y, Xie M, Reitz RD. Towards a comprehensive understanding of the influence of fuel properties on the combustion characteristics of a RCCI (reactivity controlled compression ignition) engine. Energy 2016;99:69–82. https://doi.org/10.1016/j.energy.2016.01.056.
[11] Agarwal AK, Singh AP, Maurya RK. Evolution, challenges and path forward for low temperature combustion engines. Prog Energy Combust Sci 2017;61:1–56. https://doi.org/10.1016/j.pecs.2017.02.001.
[12] Abd-Alla GH. Using exhaust gas recirculation in internal combustion engines: a review. Energy Convers Manage 2002;43:1027–42. https://doi.org/10.1016/S0196-8904(01)00091-7.
[13] Özener O, Yüksek L, Ergenç AT, Özkan M. Effects of soybean biodiesel on a DI diesel engine performance, emission and combustion characteristics. Fuel 2014;115:875–83. https://doi.org/10.1016/j.fuel.2012.10.081.
[14] Dong S, Wang Z, Yang C, Ou B, Lu H, Xu H, et al. Investigations on the effects of fuel stratification on auto-ignition and combustion process of an ethanol/diesel dual-fuel engine. Appl Energy 2018;230:19–30. https://doi.org/10.1016/j.apenergy.2018.08.082.
[15] Song R, Liu J, Wang L, Liu S. Performance and emissions of a diesel engine fuelled with methanol. Energy Fuels 2008;22:3883–8. https://doi.org/10.1021/ef800492r.
[16] Han X, Yang Z, Wang M, Tjong J, Zheng M. Clean combustion of n-butanol as a next generation biofuel for diesel engines. Appl Energy 2017;198:347–59. https://doi.org/10.1016/j.apenergy.2016.12.059.
[17] Wei L, Geng P. A review on natural gas/diesel dual fuel combustion, emissions and performance. Fuel Process Technol 2016;142:264–78. https://doi.org/10.1016/j.fuproc.2015.09.018.
[18] Chintala V, Subramanian KA. A comprehensive review on utilization of hydrogen in a compression ignition engine under dual fuel mode. Renew Sustain Energy Rev 2017;70:472–91. https://doi.org/10.1016/j.rser.2016.11.247.
[19] Gonca G, Sahin B, Parlak A, Ust Y, Ayhan V, Cesur İ, et al. Theoretical and experimental investigation of the Miller cycle diesel engine in terms of performance and emission parameters. Appl Energy 2015;138:11–20. https://doi.org/10.1016/j.apenergy.2014.10.043.
[20] Benajes J, Serrano JR, Molina S, Novella R. Potential of Atkinson cycle combined with EGR for pollutant control in a HD diesel engine. Energy Convers Manage 2009;50:174–83. https://doi.org/10.1016/j.enconman.2008.08.034.
[21] Aliabadi AA, Thomson MJ, Wallace JS, Tzanetakis T, Lamont W, Di Carlo J. Efficiency and emissions measurement of a stirling-engine-based residential microcogeneration system run on diesel and biodiesel. Energy Fuels 2009;23:1032–9. https://doi.org/10.1021/ef800778g.

[22] Amrouche F, Erickson P, Park J, Varnhagen S. An experimental investigation of hydrogen-enriched gasoline in a Wankel rotary engine. Int J Hydrog Energy 2014;39:8525–34. https://doi.org/10.1016/j.ijhydene.2014.03.172.
[23] Mikalsen R, Roskilly AP. A review of free-piston engine history and applications. Appl Therm Eng 2007;27:2339–52. https://doi.org/10.1016/j.applthermaleng.2007.03.015.
[24] Internal HJ. Combustion Engine Fundamentals. McGraw-Hill Education; 1988.
[25] Chen R, Winward E, Stewart P, Taylor B, Gladwin D. Quasi-Constant Volume (QCV) Spark Ignition Combustion. Warrendale, PA: SAE International; 2009. doi:10.4271/2009-01-0700.
[26] Dorić JŽ, Klinar IJ. Efficiency of a new internal combustion engine concept with variable piston motion. Therm Sci 2014;18:113–27.
[27] Shaik A, Moorthi NSV, Rudramoorthy R. Variable compression ratio engine: A future power plant for automobiles – an overview. Proc Inst Mech Eng Part J Automob Eng 2007;221:1159–68. https://doi.org/10.1243/09544070JAUTO573.
[28] Zhang C, Sun Z. Using variable piston trajectory to reduce engine-out emissions. Appl Energy 2016;170:403–14. https://doi.org/10.1016/j.apenergy.2016.02.104.
[29] Zhang C, Li K, Sun Z. Modeling of piston trajectory-based HCCI combustion enabled by a free piston engine. Appl Energy 2015;139:313–26. https://doi.org/10.1016/j.apenergy.2014.11.007.
[30] Zhang C, Sun Z. Trajectory-based combustion control for renewable fuels in free piston engines. Appl Energy 2017;187:72–83. https://doi.org/10.1016/j.apenergy.2016.11.045.
[31] Tsujimura T, Suzuki Y. The utilization of hydrogen in hydrogen/diesel dual fuel engine. Int J Hydrog Energy 2017;42:14019–29. https://doi.org/10.1016/j.ijhydene.2017.01.152.
[32] The Covaxe Engine, https://www.covaxe.com/the-engine/; 2020.
[33] Khan IM, Greaves G. A method for calculating the formation and combustion of soot in diesel engines. Heat Transf Flames 1974.
[34] Barths H, Antoni C, Peters N. Three-Dimensional Simulation of Pollutant Formation in a DI Diesel Engine Using Multiple Interactive Flamelets. Warrendale, PA: SAE International; 1998. doi:10.4271/982459.
[35] Patel A, Kong S-C, Reitz RD. Development and Validation of a Reduced Reaction Mechanism for HCCI Engine Simulations. Warrendale, PA: SAE International; 2004. doi:10.4271/2004-01-0558.
[36] Wang H, Deneys Reitz RD, Yao M, Yang B, Jiao Q, Qiu L. Development of an n-heptane-n-butanol-PAH mechanism and its application for combustion and soot prediction. Combust Flame 2013;160:504–19. https://doi.org/10.1016/j.combustflame.2012.11.017.
[37] Kim H, Reitz RD, Kong SC. Modelling combustion and emissions of HSDI diesel engines using injectors with different included spray angles. SAE Technical Paper; 2006; 2006-01-1150. doi:10.4271/2006-01-1150.
[38] Dimitriou P, Kumar M, Tsujimura T, Suzuki Y. Combustion and emission characteristics of a hydrogen-diesel dual-fuel engine. Int J Hydrog Energy 2018;43:13605–17. https://doi.org/10.1016/j.ijhydene.2018.05.062.
[39] Musculus MPB, Lachaux T, Pickett LM, Idicheria CA. End-of-Injection Over-Mixing and Unburned Hydrocarbon Emissions in Low-Temperature-Combustion Diesel Engines. Warrendale, PA: SAE International; 2007. doi.:10.4271/2007-01-0907.
[40] Bobba MK, Genzale CL, Musculus MPB. Effect of ignition delay on in-cylinder soot characteristics of a heavy duty diesel engine operating at low temperature conditions. SAE Int J Engines 2009;2:911–24.
[41] Hanson RK, Salimian S. Survey of Rate Constants in the N/H/O System. In: Gardiner WC, editor. Combust. Chem., New York, NY: Springer New York; 1984, p. 361–421. doi:10.1007/978-1-4684-0186-8_6.
[42] Turns SR. An Introduction to Combustion: Concepts and Applications. 3rd ed. New York: McGraw-Hill Education; 2011.
[43] Pollard JH. A Handbook of Numerical and Statistical Techniques: With Examples Mainly from the Life Sciences. CUP Archive; 1979.
[44] Thangaraja J, Kannan C. Effect of exhaust gas recirculation on advanced diesel combustion and alternate fuels – a review. Appl Energy 2016;180:169–84. https://doi.org/10.1016/j.apenergy.2016.07.096.